Applied Physics Express

LETTER

Temperature profile of nanospintronic device analyzed by spin-dependent Seebeck effect

Applied Physics Express 14, 073004 (2021)
https://doi.org/10.35848/1882-0786/ac0b05

LETTER

Temperature profile of nanospintronic device analyzed by spin-dependent Seebeck effect

Md Kamruzzaman[1,2], Shaojie Hu[1], Kohei Ohnishi[1], and Takashi Kimura[1*]

[1]Department of Physics, Kyushu University, 744 Motooka, Fukuoka, 819-0395, Japan
[2]Department of Physics, University of Dhaka, Dhaka-1000, Bangladesh

*E-mail: t-kimu@phys.kyushu-u.ac.jp

Received May 18, 2021; revised June 2, 2021; accepted June 14, 2021; published online July 2, 2021

The heat transport in a laterally configured nano-spintronic device, including a magnetic multi-layered nanowire has been investigated by detecting the second harmonic voltages. We show that the magnetic-field dependence of the second harmonic voltage in the multi-layered wire shows a clear spin-valve-like effect with the magnitude larger than the electrical spin valve effect. The second harmonic signal with its probe configuration dependence is found to be quantitatively explained by the spin-dependent Seebeck effect with a significant heat flow from the substrate. This demonstration paves the way for the precise analysis of the heat flow in nano-structured electronic devices.

Recent development of nano-fabrication techniques enable the realization of functional electronic devices with lateral dimensions down to nano-meter scale. In the operation of such nano-sized devices, understanding and controlling the heat transfer is an important issue because a small cross section produces a significant Joule heating effect. Since the characteristic lengths, such as the mean free path and phase coherent length are comparable to the device dimension, the heat transport in nano-structured systems may be different from the bulk state and its combination. On the other hand, utilizing the Joule heat through the thermal energy conversion is also an attractive and challenging issue from the viewpoint of energy harvesting.[1)]

In the field of spintronics, in addition to the intriguing spin-dependent transports,[2)] such as giant magnetoresistance (GMR), tunnel magneto-resistance and the spin Hall effect (SHE), various conversion phenomena between spin and heat such as spin Seebeck,[3)] spin Peltier,[4,5)] and spin Nernst effects[6)] have been recently reported, and a new research field has emerged; this is known as spincaloritronics.[7–12)] A key quantity for the operation of the spintronic devices is a spin current, which is the flow of spin angular momentum.[13,14)] In order to generate a large spin current, a large current density is required, leading to the large thermal energy dissipation. Thermal spin injection driven by the temperature gradient is also an attractive phenomenon for generating the spin current.[15,16)] Thus, it is essential to deepen our understanding of the heat transfer in nanospintronic devices for manipulating the heat as well as for developing spincaloritronics. In the present study, we develop an effective method for characterizing the temperature distribution in nanospintronic devices by using the magneto-Seebeck effect.[17–20)]

We have fabricated a laterally configured ferromagnetic/nonmagnetic hybrid structure, consisting of a Co/Cu/NiFe GMR wire and a Pt wire bridged by a Cu strip. Here, Pt is a representative material used in spin Hall devices, and the Co/Cu/NiFe trilayered wire is various applications such as magnetic sensor and spin-torque oscillator. Figure 1 shows a scanning electron microscope image of the fabricated device together with its schematic illustration. The device has been fabricated on a Si substrate whose surface was thermally oxidized for the formation of 1 μm thick SiO_2. Here, the GMR wire consists of NiFe (10 nm)/Cu (10 nm)/Co (10 nm) trilayed structure, which show the electrical and thermal spin valve effects. The thickness for the Pt wire and the Cu strip are 10 nm and 100 nm, respectively. Prior to the Cu deposition, the surfaces for the GMR and Pt wires were well cleaned by the Ar ion milling. The electrical resistivities for Co, NiFe, Pt and Cu are 19.3 $\mu\Omega$ cm, 33.9 $\mu\Omega$ cm, 21.8 $\mu\Omega$ cm and 2.98 $\mu\Omega$ cm at room temperature, respectively. In the present device, the Pt wire was used as an electrical heater. The generated heat propagates through the Cu strip as well as the substrate. Since the temperature change due to the Joule heating is proportional to the current square, we can effectively pick up the thermoelectric voltage by using the second-harmonic detection technique based on the Seebeck effect.[21)]

First, we evaluate the electrical transport property of the GMR wire by measuring the magnetoresistance. Here, the magnetic field is applied along the wire direction. Figure 2(a) shows the GMR property measured at room temperature. The magneto-resistance shows a clear spin valve effect where the first positive resistance change and second negative one are caused by the magnetization reversals for the NiFe and Co, respectively. Here, the normalized resistance change defined by $(R_P–R_{AP})/R_{AP}$ is approximately 0.4%. For a comparison, in Fig. 2(b), we also show the magnetoresistance for another side (lower part) of the GMR wire. The normalized resistance change is also 0.4%, which is the same as that in Fig. 1(a). This fact assures that the GMR wires on both sides have the same electrical property.

Secondly, the heat transport properties under the Joule heating of the Pt wire is evaluated. We flow an ac current from the Pt wire to the Cu strip and measure the second-harmonic voltage between the GMR wire and Cu strip. Here, the second-harmonic signals is obtained by averaging it 30 times. From the viewpoint of the Seebeck voltage, we naively expected that the detected voltage is proportional to the temperature at the junction between the GMR wire and Cu strip. Figure 3(a) shows the field dependence of the second-harmonic signal with the bias current of 0.54 mA. When the base voltage is negative and we see a clear spin valve effect, where the parallel state provides a larger voltage than that for the anti-parallel state. Figure 3(b) shows the bias current dependence of the second-harmonic voltage for the parallel and anti-parallel state. Clear parabolic behaviors have been obtained, assuring that the signal is caused by the Joule

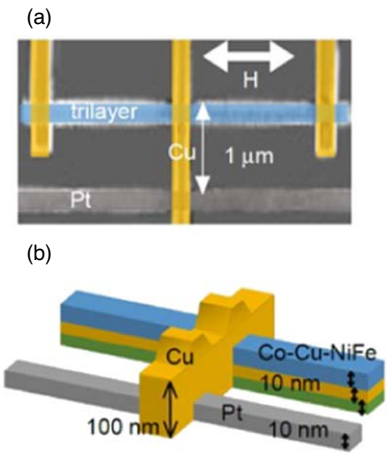

Fig. 1. (Color online) (a) Scanning electron microscope image and (b) schematic illustration of the fabricated device, consisting of a Co/Cu/NiFe GMR wire and a Pt wire bridged by a nonmagnetic Cu strip. The magnetic field is applied along the GMR wire direction.

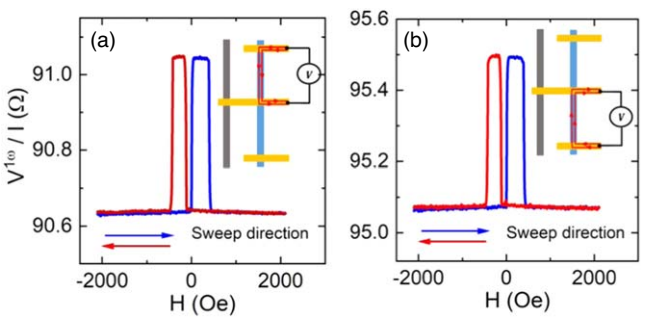

Fig. 2. (Color online) Field dependence of the electrical resistance for the upper (a) and lower GMR wire (b). The probe configurations are shown in the inset of each figure. The blue and red curves correspond to forward and backward field sweeps, respectively.

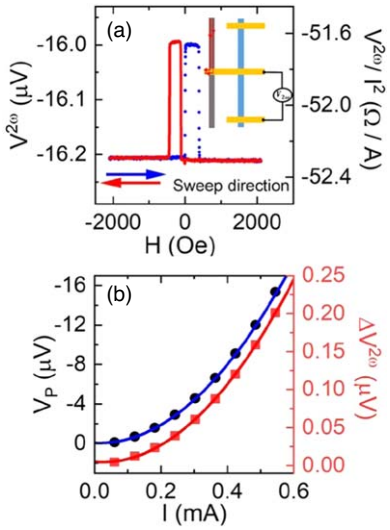

Fig. 3. (Color online) (a) Field dependence of second harmonic signal for the GMR wire under Joule heating of the Pt wire to the Cu strip. The inset shows the probe configuration for the measurement. (b) Bias current dependence of the second harmonic signal at the parallel state and the voltage change between the parallel and anti-parallel state. The solid line corresponds to the fitted curve with a parabolic dependence.

heating.[16] Here, the negative background voltage is qualitatively understood by relatively large negative Seebeck coefficients for the ferromagnetic metals.[22–24] Interestingly, the normalized voltage change defined by $(V_P–V_{AP})/V_{AP}$ is 1.3%, which is more than three times the electrical GMR ratio. This means that the spin polarization for the Seebeck coefficient is larger than that for the electrical conductivity and indicates a high potential application of the giant-magneto Seebeck effect for the energy conversion and heat control in nano-structured devices.

We then study the probe configuration dependence of the second-harmonic signal. Since the upper-side and lower-side GMR wires show the same electrical transport properties, we naively expect that a similar second-harmonic voltage is observed by using the left-hand-side GMR wire as a V_+ terminal. Figure 4(a) shows the field dependence of second-harmonic signal with the probe configuration shown in the inset. Surprisingly, the base voltage was much smaller than that with the previous configuration. In addition, the inverse thermal spin valve signal has been observed. To understand this discrepancy more clearly, we have changed I_+ terminal from the upper-side to the lower-side Pt wire as schematically shown in the inset of Fig. 4(b). Interestingly, we were able to observe a large second-harmonic voltage with the clear thermal spin valve effect, similarly in Fig. 3(a). As a further experiment, we have also measured the second-harmonic signal with the probe configuration shown in the inset of Fig. 4(c) and observed a small voltage signal similarly to Fig. 4(a). These results clearly indicate that the location of the heating area plays a significant role in the second-harmonic voltage.

In order to understand these unexpected behaviors, we have performed a COMSOL numerical simulation with carefully taking into account the heat conduction from the substrate. In the simulation, the heat conductivities for the metallic wires were simply estimated from Wiedemann–Franz law with their actual electrical conductivities.[25] On the other hand, we adopt the bulk heat conductivities for Si and SiO_2 layers, which are 147.62 W mK^{-1} and 1.38 W mK^{-1}. Figure 5(a) shows the simulation result for the temperature distribution around the junction under the Joule heating of the Pt wire. Here, we label the average temperature around upper, center and lower Cu/GMR junctions as T_1, T_2 and T_3, respectively. In the present condition, since the heat mainly flows through the metallic wire, the temperature in the GMR wire takes a maximum value at the center junction with the Cu strip, namely T_2 To understand the temperature distribution in the GMR wire, we have prepared the line profile of the temperature along the GMR wire, as shown in Fig. 5(c). It should be noted that T_1, which is located in the same side of the Pt heater, is higher than T_3, meaning $T_2 > T_1 > T_3$. However, the temperature difference between T_2 and T_1 is much smaller than the difference between T_2 and T_3. This means that the heat flow from the substrate is non-negligible. Since the output voltage in the second-harmonic detection is proportional to the temperature difference between the center and edge position, this indicates that a small Seebeck voltage is induced in the probe configuration for the inset of Figs. 4(a) and 4(c). However, as seen in Figs. 4(a) and 4(c), the negative Seebeck voltage and

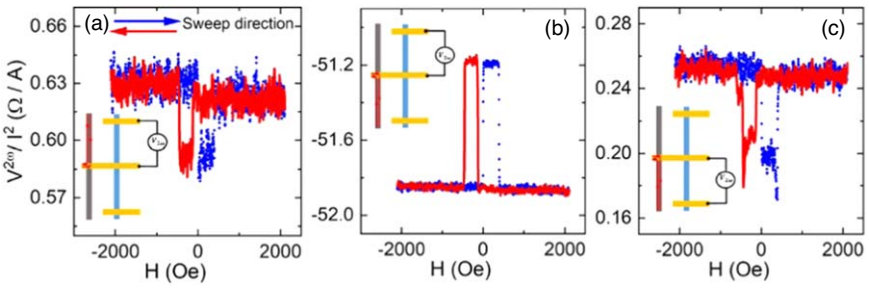

Fig. 4. (Color online) Field dependence of thermal spin valve signal with various probe configurations are shown in (a), (b) and (c). Here, the voltage is detected at the same probes in (a) and (b), only I_+ terminal has changed from the upper-side to the lower-side Pt wire in (b). I_+ and I_- terminals are in the same position in (b) and (c) where V_+ terminal has changed from the upper-side to lower-side GMR wire in (c).

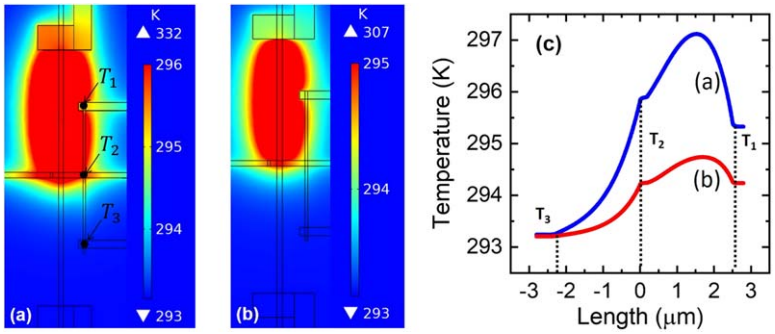

Fig. 5. (Color online) Numerically obtained temperature distribution around the GMR wire under a bias current of 0.55mA in the Pt simulated with the bulk heat conductivity of SiO_2 (a) and the enhanced heat conductivity of SiO_2 with the factor of 2.5 (b). T_1, T_2 and T_3 are the average temperature around upper, center and lower Cu/GMR junctions of the device. (c) Line profile of the temperature distribution along the GMR wire for the bulk heat conductivity and enhanced heat conductivity for SiO_2

inverse voltage change cannot be explain by the present numerical results.

Based on this simulated result, we increased the heat conductivity of the SiO_2 layer with the factor of 2.5. Figure 5(b) shows the temperature distribution around the junction under the revised condition. Importantly, we are able to reproduce the sign reversal of the Seebeck voltage, as shown in Figs. 5(b) and 5(c), meaning the relation $T_1 > T_2 > T_3$. Here, temperature T_1, T_2 and T_3 are 294.243 K, 294.231 K and 293.255 K, respectively. We emphasize that the ratio between T_1–T_2 and T_3–T_2 is approximately 80, which is the same as the ratio of the Seebeck voltage for two probe configurations. This indicates that the simulated results with the modified heat conductivity represents a more realistic situation. We believe that the large heat conductivity for SiO_2 is not unrealistic situation because of various extrinsic effects such as the formation of the mixing layer between the metal and SiO_2 interface and the partial formation of SiO_x. If we adopt the simulated results, we are able to estimate the Seebeck coefficients for the GMR wire $S^{\mathrm{P}}_{\mathrm{GMR}}$ and $S^{\mathrm{AP}}_{\mathrm{GMR}}$ as $-15.87\,\mu\mathrm{V\,K^{-1}}$ and $-15.67\,\mu\mathrm{V\,K^{-1}}$, respectively. The values are close to the ferromagnetic metals, supporting the validity of the numerical simulation.[22–24] We also emphasize that the reliability of the 2nd harmonic voltage is confirmed both from the sign reversal of the voltage and the ratio of the thermal spin valve effect.

In conclusion, we have investigated a heat transport in a laterally configured nano-spintronic device consisting of a GMR nanowire and a Pt nanowire bridged by a Cu strip. The heat flow produced by a Joule heating in a Pt wire is analyzed by detecting the second harmonic voltage in the GMR wire. The second harmonic voltage in the GMR wire shows a clear thermal spin valve effect whose magnitude is three times larger than the electrical GMR effect. From the probe configuration dependence of the second harmonic signal, we find that the heat flow from the substrate is more significant than the expected. The combination between the thermoelectric effect and spin-dependent transport provides an effective analysis of the heat transport in nanospintronic devices.

Acknowledgments This work is partially supported by Grant-in-Aid for Scientific Research (A)(18H03866), Grant-in-Aid for Challenging Research (Pioneering)(17H06227) and JST CREST (JPMJCR18J1).

1) R. Venkatasubramanian, "Nanothermal trumpets," Nature **463**, 619 (2010).
2) I. Žutić, J. Fabian, and S. Das Sarma, "Spintronics: fundamentals and applications," Rev. Mod. Phys. **76**, 323 (2004).
3) K. Uchida, S. Takahashi, K. Harii, J. Ieda, W. Koshibae, K. Ando, S. Maekawa, and E. Saitoh, "Observation of the spin Seebeck effect," Nature **455**, 778 (2008).
4) J. Flipse, F. L. Bakker, A. Slachter, F. K. Dejene, and B. J. Van Wees, "Direct observation of the spin-dependent Peltier effect," Nat. Nanotechnol. **7**, 166 (2012).
5) J. Flipse, F. K. Dejene, D. Wagenaar, G. E. W. Bauer, J. Ben Youssef, and B. J. van Wees, "Observation of the spin Peltier effect for magnetic insulators," Phys. Rev. Lett. **113**, 027601 (2014).
6) S. Meyer et al., "Observation of the spin Nernst effect," Nat. Mater. **16**, 97 (2017).
7) G. E. W. Bauer, A. H. MacDonald, and S. Maekawa, "Spin caloritronics," Solid State Commun. **150**, 459 (2010).
8) M. Johnson, "Spin caloritronics and the thermomagnetoelectric system," Solid State Commun. **150**, 543 (2010).
9) G. E. W. Bauer, E. Saitoh, and B. J. van Wees, "Spin caloritronics," Nat. Mater. **11**, 391 (2012).
10) S. R. Boona, R. C. Myers, and J. P. Heremans, "Spin caloritronics," Energy Environ. Sci. **7**, 885 (2014).

11) H. Yu, S. D. Brechet, and J. P. Ansermet, "Spin caloritronics, origin and outlook," Physics Letters, Section A: General, Atomic and Solid State Physics **381**, 825 (2017).
12) K.-I. Uchida, "Transport phenomena in spin caloritronics," Proceedings of the Japan Academy, Series B **97**, 69 (2021).
13) S. Maekawa et al., *Concepts in Spin Electronics* (Oxford University Press, Oxford, 2006), vol 13.
14) S. Maekawa, S. O. Valenzuela, T. Kimura, and E. Saitoh, *Spin Current* (Oxford University Press, Oxford, 2017).
15) A. Slachter, F. L. Bakker, J. P. Adam, and B. J. Van Wees, "Thermally driven spin injection from a ferromagnet into a non-magnetic metal," Nat. Phys. **6**, 879 (2010).
16) S. Hu, H. Itoh, and T. Kimura, "Efficient thermal spin injection using CoFeAl nanowire," NPG Asia Mater. **6**, e127 (2014).
17) L. Gravier, S. Serrano-Guisan, F. Reuse, and J.-P. Ansermet, "Thermodynamic description of heat and spin transport in magnetic nanostructures," Phys. Rev. B **73**, 024419 (2006).
18) S. Jain, D. D. Lam, A. Bose, H. Sharma, V. R. Palkar, C. V. Tomy, Y. Suzuki, and A. A. Tulapurkar, "Magneto-Seebeck effect in spin-valve with in-plane thermal gradient," AIP Adv. **4**, 127145 (2014).
19) X. M. Zhang, C. H. Wan, H. Wu, P. Tang, Z. H. Yuan, Q. T. Zhang, X. Zhang, B. S. Tao, C. Fang, and X. F. Han, "Magneto-Seebeck effect in spin valves," J. Appl. Phys. **122**, 145105 (2017).
20) S. Chen, Z. Yang, Y. Zuo, M. Si, L. Xi, H. Shi, D. Yang, and D. Xue Temperature, "dependence of the electrical and thermal transport in FeCo/Cu/$Ni_{80}Fe_{20}$ spin valves," J. Phys. D. Appl. Phys. **51**, 40 (2018).
21) S. Hu, T. Nomura, G. Uematsu, N. Asam, and T. Kimura, "First- and second-harmonic detection of spin accumulation in a multiterminal lateral spin valve under high-bias ac current," Phys. Rev. B **94**, 014416 (2016).
22) F. L. Bakker, J. Flipse, and B. J. Van Wees, "Nanoscale temperature sensing using the Seebeck effect," J. Appl. Phys. **111** (2012).
23) C. Mu, S. Hu, J. Wang, and T. Kimura, "Thermo-electric effect in a nano-sized crossed Permalloy/Cu junction under high bias current," Appl. Phys. Lett. **103**, 132408 (2013).
24) S. J. Mason, A. Hojem, D. J. Wesenberg, A. D. Avery, and B. L. Zink, "Determining absolute Seebeck coefficients from relative thermopower measurements of thin films and nanostructures," J. Appl. Phys. **127**, 085101 (2020).
25) A. D. Avery, S. J. Mason, D. Bassett, D. Wesenberg, and B. L. Zink, "Thermal and electrical conductivity of approximately 100-nm permalloy, Ni, Co, Al, and Cu films and examination of the Wiedemann-Franz law," Physical Review B **92**, 214410 (2015).